
PROCEEDINGS OF THE
18TH WORLD CONFERENCE ON EARTHQUAKE ENGINEERING
WCEE2024
MILAN

18TH WORLD CONFERENCE ON EARTHQUAKE ENGINEERING
WCEE2024
MILAN

MILAN, ITALY
30TH JUNE - 5TH JULY 2024

www.wcee2024.it

SENSITIVITY ANALYSIS OF DOUBLE-INTERFACE ROCKING WALLS WITH ADDITIONAL HYSTERETIC AND VISCOUS DAMPERS

Simone Labò[1], Ameer Marzok[2], Andrea Belleri[1], Oren Lavan[3], Michele Bianchessi[1]

[1] University of Bergamo, Bergamo, Italy, andrea.belleri@unibg.it

[2] Columbia University, New York, USA

[3] Technion - Israel Institute of Technology Technion, Haifa, Israel

Abstract: *Several researchers have investigated the seismic efficiency of rocking systems with multiple rocking interfaces, which are suitable for both new buildings and retrofits of existing buildings. In this paper, the seismic performance of double rocking systems with additional hysteretic and viscous devices is evaluated. In particular, the investigated solution considers an additional bracing system above the second rocking interface to control the seismic damage to drift-prone elements.*
So far, only the effectiveness of such a system has been investigated with hysteretic devices (i.e., structural steel bars attached to the rocking interfaces). This paper presents the results of a sensitivity analysis that investigated the different ways in which hysteretic and viscous devices can be used together through non-linear response history analyses for a reference case study.

1. Introduction

Rocking systems have been widely studied and significant benefits have been observed when these systems are used in both new buildings and retrofit of existing buildings (Kurama et al. 1999; Holden et al. 2003; Perez et al. 2013; Restrepo and Rahman 2007; Pennucci et al. 2009). These structures may be designed to concentrate damage in localised and easily repaired elements such as external dissipative elements, which may be, for example, hysteretic (Rahman et al. 2000; Kurama et al. 1999; Schoettler et al. 2009; Belleri et al. 2015), viscous (Marriott et al. 2008; Pollino 2015) or frictional (Rahman et al. 2000; Christopoulos et al. 2002; Tremblay et al. 2008). Energy dissipation also leads to a reduction in base shear and ground accelerations, which are considered crucial in the design of retrofit solutions. Gravity loads and unbonded post-tensioned tendons re-centre the structure after an earthquake, reducing or even avoiding residual displacements.

In this context, the seismic behaviour of double rocking systems equipped with an additional bracing system above the second rocking interface was investigated in order to control seismic damage to vibration-prone elements. So far, only the effectiveness of such a system with hysteretic devices (i.e. with structural steel bars attached to the rocking interfaces) has been investigated. In this work, the response of the system when hysteretic and viscous devices are used together has been investigated using a finite element model and numerical analysis. A peculiar characteristic of this system is the pure horizontal translation of the building above the second rocking interface, therefore avoiding damage in drift-sensitive structural and non-structural elements in that region. In this work, the hypothesis of perfect translation was maintained by limiting the inter-story drift to be equal to or less than 1/10 of the inter-story drift of the bi-rocking wall.

2. Effect of supplemental viscous damping

2.1. Methodology

In order to make some considerations on the effects of introducing viscous dampers, sensitivity analyses were first performed by varying the percentages of hysteretic (H) and viscous (V) dissipation amount point by point, starting from the case where the dissipated energy is provided by hysteretic devices (100%H-0%V) to the case

where it is provided only by viscous dampers (0%H-100%V). Parametric analyses were then performed using a numerical model previously developed by Marzok and Lavan (2021), allowing the investigation of the optimal combination of pre-tension force, hysteretic and viscous energy quantity to be determined.

2.2. Reference building and double-rocking interface system layout

To design the double-rocking interface system, and the sensitivity and parametric studies, reference was made to a typical 6-story RC building, 18m tall and with a (12x18) m^2 rectangular plan (Mpampatsikos et al. 2020). The structure is supposed in a high seismicity area: design spectrum for Eurocode 8 (CEN 2005) with soil class C, topography T1, and ground acceleration on rock a_g equal to 0.261g.

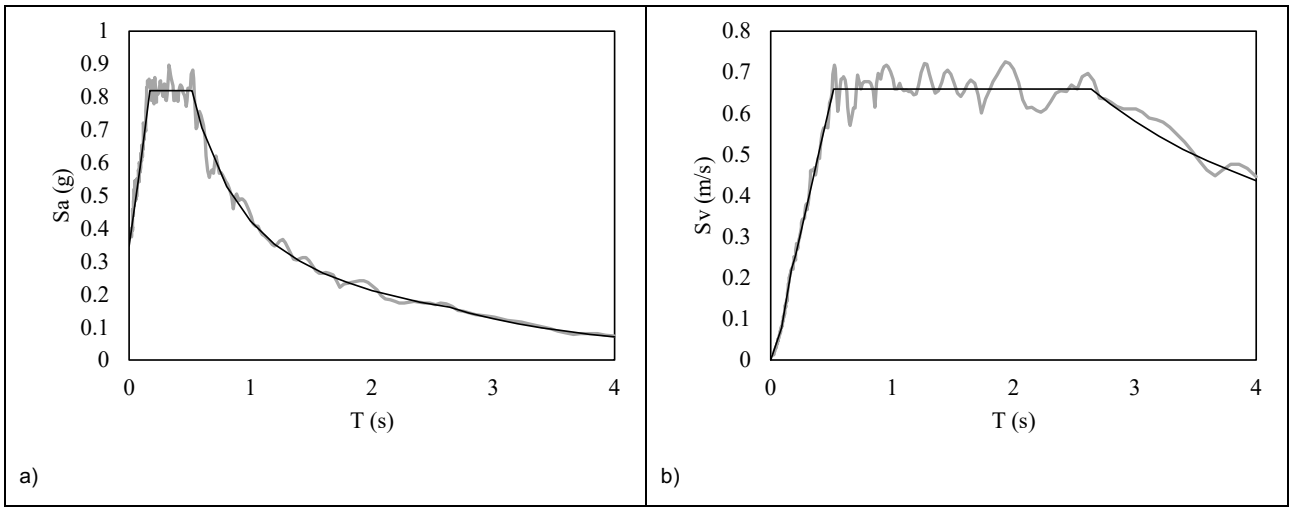

Figure 1. Design spectrum: a) pseudo acceleration as a function of the period; b) pseudo velocity as a function of the period.

Four rocking systems were considered: one at each side of the rectangular plan. In this work, a single wall-frame system was considered. The dead and live loads are 8.60 kN/m^2 and the tributary area of the considered frame is about 108 m^2. The floor tributary mass is 92880 kg.

The considered structural materials properties are summarized in Table 2 and are concrete with a cylindrical strength equal to 50 MPa, steel reinforcement with yield strength equal to 455 MPa, and post-tensioning tendons with a nominal tensile strength equal to 1860 MPa. The rocking walls were in S355 ($f_{yd,W}$=355 MPa) steel.

Table 1. Materials

Description	Symbol	Value	Unit
PT yielding stress	$f_{yd,PT}$	1670	MPa
PT ultimate stress	$f_{u,PT}$	1860	MPa
PT Elastic Modulus	$E_{s,PT}$	195000	MPa
PT yielding strain	$\varepsilon_{yd,PT}$	0.856	%
Rocking wall (RW) steel	$f_{yd,W}$	355	MPa
RW steel Elastic Modulus	$E_{s,W}$	210000	MPa

The design of the double-rocking interface system was based on the following assumptions:

1. Rocking interfaces were developed at the ground and second floors. Height of the first rocking segment (h_R) 6 m.
2. Design drift target (ϑ_d) equal to 2% (according to the Eurocode 8 (CEN 2005)). The target displacement (Δ_d) is therefore 0.12 m at the top of the first rocking segment.
3. Residual displacements must be avoided.

4. Maximum inter-story drift above the second floor (above the second rocking interface) equal or less than 0.2%.

The layout and the geometry derived from the design of the retrofit solution are depicted in Figure 2. The double-rocking interface system is made of a 3.08m steel truss in which the rocking interfaces develop at the ground and second floors; an additional bracing system above the second rocking interface was introduced and pinned with other two steel bracing systems to allow the activation of the rocking motion while controlling the seismic damage to drift-prone elements. The lateral bracing elements are supported by trusses. Figure 2b reports the geometry of the elements.

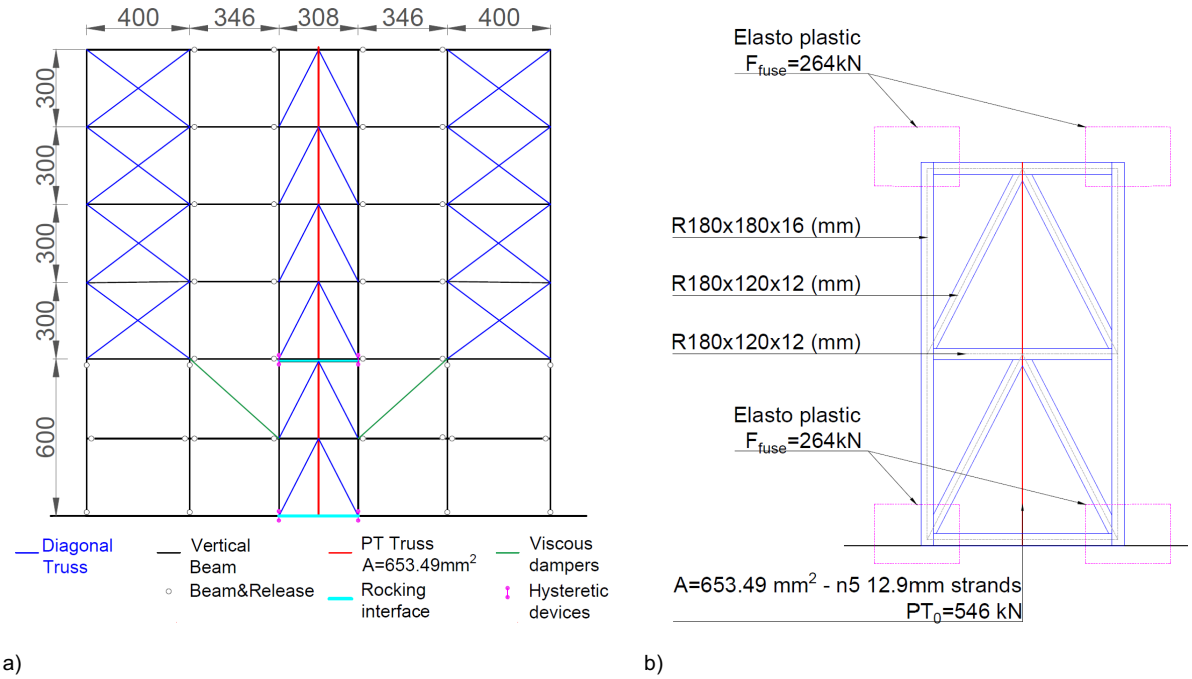

a) b)

Figure 2. a) Layout of the retrofit solution (dimension in cm); b) Detail of the rocking wall and element dimensions.

The post-tensioning cable has a cross-sectional area of 653 mm^2 and develops unbounded along the entire height. The design procedure indicated that the initial prestress required to meet the design objectives was 546 kN, while the hysteretic devices were designed according with available literature (Kurama et al. 1999, Rahman et al. 2000). A λ value equal to 1.6 was adopted where λ is the ratio between the re-centring contribution deriving from the post tensioning cable, and the contribution of the hysteretic devices. The wall self-weight was neglected. Accordingly, the activation force of the hysteretic devices (F_{HD}) placed at the corners of the rocking interfaces was 264 kN. The ratio between the elastic moment at the rocking section to the decompression moment consisting of contributions from moments due to post-tensioned cables, and hysteretic energy dissipators (defined as R in the following Section) is equal to 3.2.

For clarity, the hysteretic devices (H) were designed without considering the viscous dampers (V); this was the case where 100% of the dissipation energy was provided by hysteretic devices (this case is referred to as 100%H-0%V in section 2.3).

When the viscous dampers were considered, they were strategically placed at the interface between the second and third floors, as shown in Figure 1. This placement was chosen because greater displacements and velocities between floors were expected in this area. The viscous devices were initially designed to dissipate the same amount of energy obtained from the use of hysteretic devices. To calculate the amount of energy dissipated by the hysteretic devices, a quasi-static non-linear analysis was performed up to the target displacement. From the energy equivalence, a damping coefficient C of 2184kNs/m was determined for linear viscous dampers. When viscous dampers with a damping coefficient C of 2148kNs/m were introduced in the

parametric analyses, the hysteretic devices were removed (this case is referred to as 0%H-100%V in section 2.3).

2.3. Sensitivity analysis

Time history analyses were conducted to evaluate the effectiveness of the design and to assess the impact of introducing viscous dampers. One Ground motion compatible with the design response spectrum was considered according to the site parameters presented in Section 2.2. Figure 1 shows how the compatible ground motion fits with the design spectrum. The double-rocking interface system was modelled using MidasGen software (MidasGen, 2020). Vertical and horizontal elements were modelled as elastic beam elements, while the diagonals were truss elements. Rotation constraints were released in the horizontal elements connecting the double-rocking interface system to the side lateral bracing system. The floor masses were modelled with nodal masses. The PT cable was modelled with an elastic truss element; the hysteretic devices were modelled with elastoplastic members, while a linear dashpot was considered for the viscous dampers. The rocking interfaces were modelled with general links that respond only to compression loads. To evaluate the influence of the introduction of viscous dampers on the structural response of the system, the amount of energy dissipated by the hysteretic devices and viscous dampers was varied according to the cases listed in Table 2.

Table 2. Materials

Case	Description	
100%H 0%V	Dissipated energy (DE) provided by hysteretic devices	$\mathrm{F_{HD}} = 264kN, C = 0\frac{kNs}{m}$
75%H 25%V	75% of DE provided by hysteretic devices and 25% by viscous dampers	$\mathrm{F_{HD}} = 198kN, C = 246\frac{kNs}{m}$
50%H 50%V	50% of DE provided by hysteretic devices and 50% by viscous dampers	$\mathrm{F_{HD}} = 132kN, C = 1092\frac{kNs}{m}$
25%H 75%V	25% of DE provided by hysteretic devices and 75% by viscous dampers	$\mathrm{F_{HD}} = 66kN, C = 1638\frac{kNs}{m}$
0%H 100%V	Dissipated energy (DE) provided by viscous dampers	$\mathrm{F_{HD}} = 0kN, C = 2184\frac{kNs}{m}$

For each case, time history analyses were carried out. The results expressed in terms of maximum drift at the top of the double-rocking wall, base shear, and axial forces in vertical and diagonal elements are plotted in Figure 3. In Figure 3, the graphs show the effects of removing both hysteretic and viscous devices. It is worth noting that in such a case, the rocking wall was not redesigned accordingly. The drift above the second rocking interface was not plotted; however, the maximum drift did not exceed the 0.2% imposed.

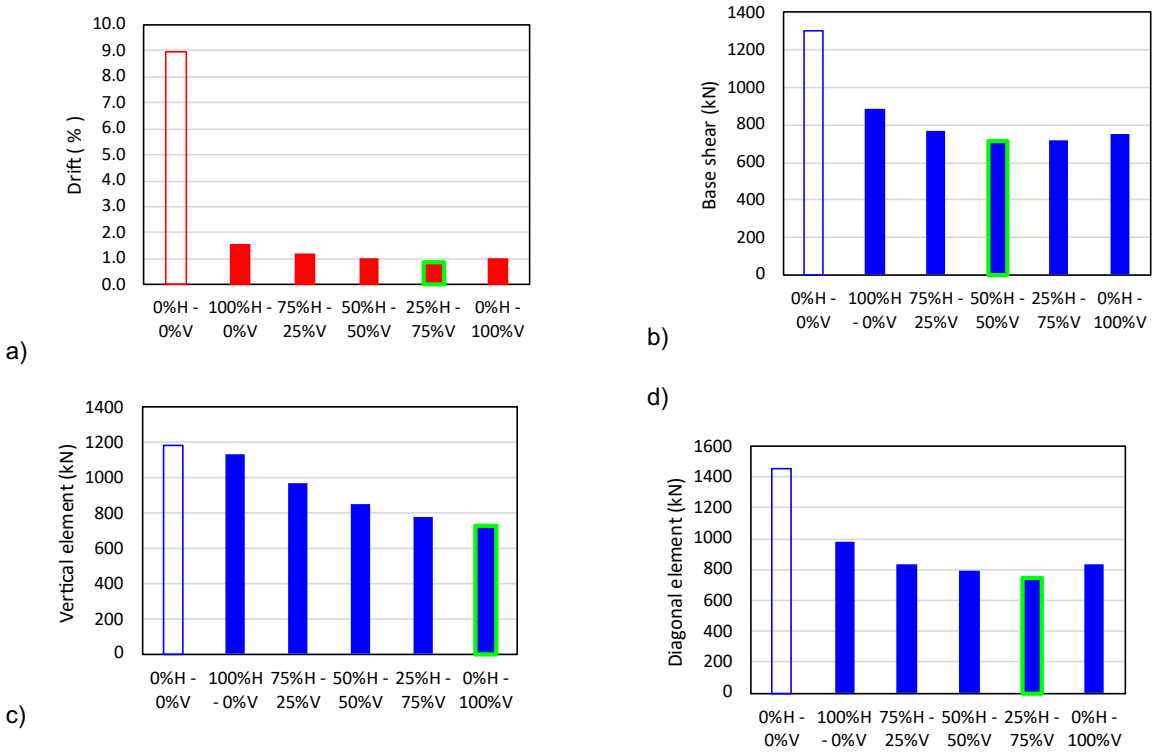

Figure 3. Results of the Time History analyses in terms of a) maximum drift, b) maximum base shear, c) and d) maximum axial force in the vertical and diagonal elements, respectively.

The results show that in all cases in which a dissipative device was introduced the target drift (2%) was achieved. The introduction of a dissipative device significantly reduces the maximum drift and base shear. The maximum drift and base shear were observed when the dissipated energy was provided only by hysteretic devices; 1.6% and 900 kN were observed, respectively. The configuration where the displacement at the top was the lowest was the 25%H-75%V configuration, where a maximum drift at the top of the rocking wall of 0.9% was observed. Base shear was lowest for the 50%H-50%V configuration (-22% compared to 100%H-0%V).

The axial force was always lower than the capacity of the elements except for the axial force observed in the diagonal element when no dissipative devices was introduced; in particular, axial capacities equal to 1728 kN and 1326 kN were calculated for vertical and diagonal elements, respectively. In the vertical elements decreased while the dissipated energy provided by the viscous dampers increased. When all the energy was dissipated by viscous dampers (0%H-100%V), the axial force in the elements decreased by about 47% compared to the 100%H-0%V case. The force in the diagonals was minimised in the 25%H-75%V case, where a reduction of 22% was observed. The introduction of viscous dampers can lead to a significant improvement in the structural response of double-rocking interface systems. However, a proportional correlation between the amount of energy dissipated by viscous dampers and the observed results cannot be established. It may be interesting to investigate whether combinations can be defined where the addition of viscous dampers leads to a reduction in all engineering demand parameters; such a problem is tentatively addressed in Section 2.4.

2.4. Parametric study

A parametric study was conducted to investigate the effect of incorporating supplemental linear viscous dampers into the system shown in Figure 2 aiming to assess optimal combination between hysteretic and viscous devices. Moreover, in this section, the influence of the required decompression moment was investigated. The structural performance was investigated by considering different reduction factors (R), ratios of plastic energy dissipation (β), and supplemental viscous dampers (considered with the damping coefficient C).

The force reduction factor is computed as the ratio between the elastic moment at the rocking section to the decompression moment, as follows:

$$R = \frac{M_{elastic}}{M_R} \quad (1)$$

Where $M_{elastic}$ is the total moment at the base of the frame when there is no rocking at the base and linear elastic behaviour is modelled for all elements.

M_R is the decompression moment consisting of contributions from moments due to post-tensioned cables, gravitational loads, and hysteretic energy dissipators computed as follows:

$$M_R = M_w + M_{PT} + M_{ED} \quad (2)$$

Where M_w, M_{PT} and M_{ED} are the moments due to gravity, post-tensioned, and the moment resulting from the hysteretic energy dissipators at the rocking section, respectively.

The parameter β is computed based on the ratio between the moment due to the hysteretic dampers and the moment due to the rocking:

$$\beta = \frac{2M_{ED}}{M_R} \quad (3)$$

This investigation encompasses a range of reduction factors from 2 to 20, as well as various ratios of plastic energy dissipation. Hysteretic dampers, with elastoplastic behaviour, were designed at the rocking sections to achieve plastic energy dissipation. The sectional areas of these elements were determined to provide different dissipation values ranging between zero and one. The former corresponds to a system without hysteretic dampers, while the latter represents a system approaching the limit of self-centring behaviour loss.

The linear viscous dampers were added at the connection between the second and third floors, as shown in Figure 2 and the damping coefficients of these elements and a summary of the parameters used in the parametric study are given in Table. 3.

Table 3. Values used in the parametric study.

Parameter	Investigated values
Reduction factor, R	2 to 20 with equal steps of 1
Plastic energy dissipation, β	0 to 1 with equal steps of 0.1
Damping coefficient, C , in $[kN \cdot sec/m]$	0,100,500,1000,5000,10000

The building was subjected to the set of ground accelerations given in (Marzok and Lavan 2023). The analyses were conducted using a numerical model previously developed by Marzok and Lavan (2021) implementing the efficient Mixed Lagrangian Formalism (Sivaselvan and Reinhorn 2006).

The results are presented in contour maps that display the mean maximum values of inter-story drifts, accelerations, displacements, forces in the columns, and forces in the braces of the self-centring frame, as shown in Figure 4, Figure 5, Figure 6, Figure 7, and Figure 8, respectively.

In general, the results show that in order to reduce the inter-story drifts and displacements, one can either decrease the value of the reduction factor, R, or alternatively, design supplemental viscous dampers. In addition, it is interesting to note that certain values of β and R exist for which the addition of viscous dampers leads to a reduction in all the engineering demand parameters (e.g. $\beta = 0.6$ with $R = 4$).

Figure 4 shows that for reduction factors higher than approximately 11 and damping coefficients less than $5000\ [kN \cdot s/m]$, the ratio of plastic energy dissipation, β, has a significant impact on the maximum inter-story drifts. Conversely, for reduction factors less than 11 or of damping coefficients larger than $5000\ [kN \cdot s/m]$, the influence of β on interstory drifts becomes less pronounced. In these cases, a reduction in the inter-story drifts can be achieved through the design of supplemental viscous damping. This example demonstrates the

effectiveness of controlling maximum inter-story drifts through supplemental viscous dampers compared to hysteretic dissipators, especially when dealing with larger reduction factors.

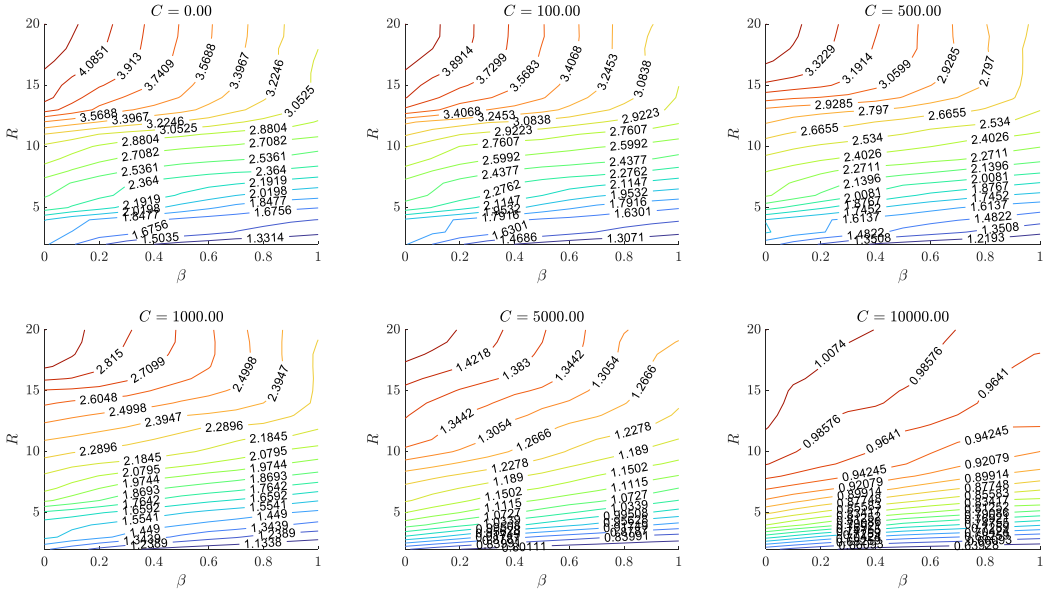

Figure 4. Mean maximum interstory drifts [%].

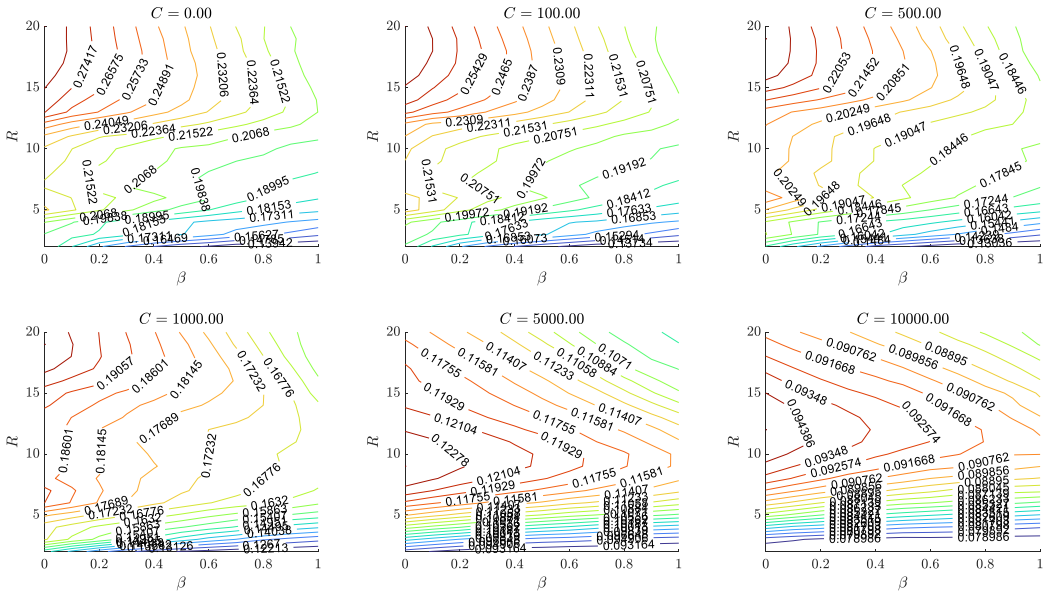

Figure 5. Mean maximum displacements [m].

Figure 5 shows that for damping coefficients below $1000\ [kN \cdot s/m]$, the maximum displacement becomes less responsive to changes in the reduction factor when the latter exceeds 8. In contrast, for high damping values ($C_d > 5000\ [kN \cdot s/m]$), there is a peak in the displacement values around reduction factors of approximately 10.

Figure 6 shows that an increase in the reduction factor, the amount of plastic energy dissipation, and the level of supplemental damping lead to a reduction in maximum accelerations. In Figure 7, it is evident that increasing the reduction factor and the amount of plastic energy dissipation results in reduced forces in the columns. For

smaller reduction factors, the increase in supplemental damping reduces these forces, while the impact of plastic energy dissipators is less pronounced. Figure 8 shows that for reduction factors greater than 4, the amount of viscous damping slightly raises the forces in the brace elements. Conversely, the opposite trend is observed for smaller reduction factors.

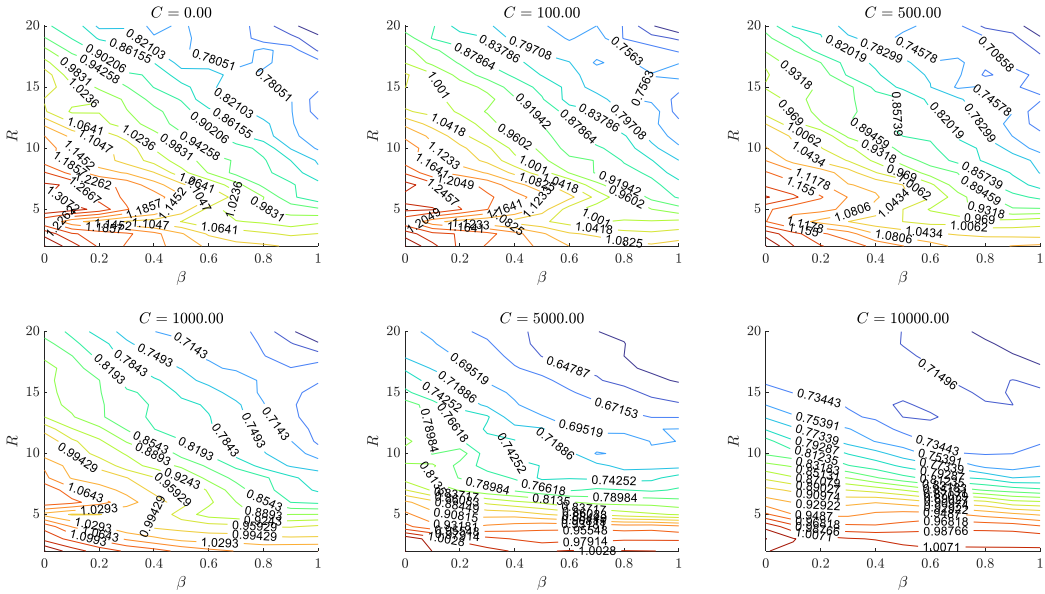

Figure 6. Mean maximum floor accelerations [m/s^2].

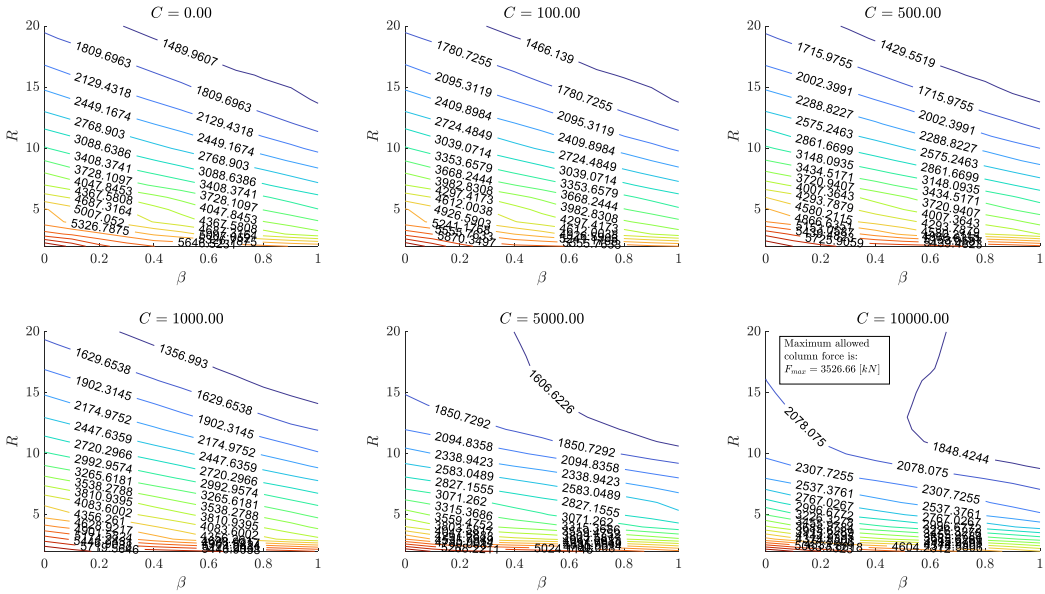

Figure 7. Mean maximum column forces of the SC-CBF in [kN].

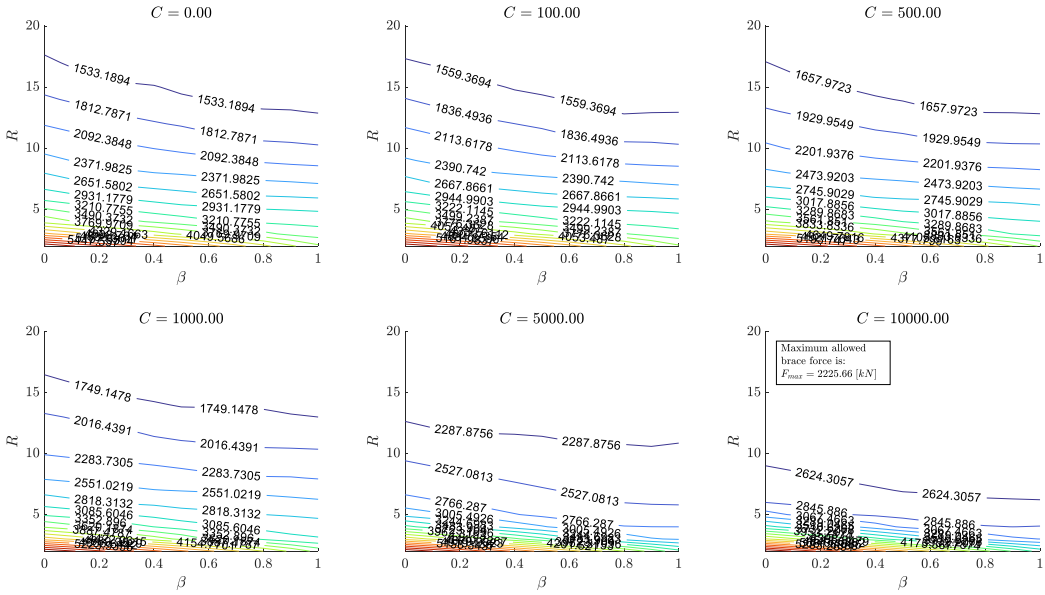

Figure 8. Mean maximum brace forces of the SC-CBF in [kN].

3. Conclusions

The effect of additional viscous damping in double-interface rocking walls was investigated. Sensitivity analyses were performed combining different percentages of hysteretic (H) and viscous (V) damping, from the case where the dissipated energy is provided by hysteretic devices (100%H-0%V) to the case where only viscous dampers were considered (0%H-100%V). From the results, it appears that the introduction of viscous dampers can lead to a significant improvement in the structural response of double-rocking interface systems.

The maximum observed reduction was about 44% and 22% with respect to the maximum drift at the top of the rocking wall and base shear, respectively. However, a linear correlation between the amount of additional viscous damping and the observed reductions cannot be established. The results were then generalised and extended by a parametric analysis using a numerical model. Different reduction factors (R - i.e. different decompression moment), ratios of plastic energy dissipation (β) and additional viscous damping (C) were considered and varied in specific areas of interest. The results show that the maximum drift can be reduced by introducing viscous dampers or increasing the decompression moment. In addition, the main finding was that there may be certain values of β and R for which the use of viscous dampers leads to a reduction in all the relevant parameters (e.g. β=0.6 with R=4).

4. References

Belleri, A., Schoettler, M.J., Restrepo, J.I., Fleishman, R.B. (2014). Dynamic behavior of rocking and hybrid cantilever walls in a precast concrete building, *ACI Structural Journal*, 111(3):661-672.

C., Filiatrault, A., Folz, B. (2002). Seismic response of self-centring hysteretic SDOF systems, *Earthquake Eng Struct Dynamics*, 31(5): 1131-1150. Doi:10.1002/EQE.152.

EC8; Eurocode 8: Design of Structures for Earthquake Resistance. European Committee for Standardization, CEN: Brussels, Belgium, 2005.

Holden, T., Restrepo, J.I., Mander, J.B. (2003). Seismic performance of precast reinforced and prestressed concrete walls, *Journal of Structural Engineering*. 129(3):286296. Doi:10.1061/(ASCE)0733-9445(2003)129:3(286).

Kurama, Y.C., Sause, R., Pessiki, S., Lu, L.W. (1999). Lateral load behavior and seismic design of unbonded post-tensioned precast concrete walls, *Struct J*, 96(4):622-632. Doi:10.14359/700.

Marriott, D., Pampanin, S., Bull, D., Palermo, A. (2008). Dynamic testing of precast, post-tensioned rocking wall systems with alternative dissipating solutions, *Bulletin of the New Zealand Society for Earthquake Engineering*. Doi:10.5459/bnzsee.41.2.90-103.

Marzok, A., & Lavan, O. (2021). Mixed Lagrangian formalism for dynamic analysis of self‐centering systems. Earthquake Engineering & Structural Dynamics, 50(4), 998-1019.

Marzok, A., & Lavan, O. (2023). Optimal Seismic Design of Controlled Coupled Multiple Rocking Systems with Viscous Dampers in Irregular Buildings. Journal of Structural Engineering, 149(2), 04022232.

MidasGEN. Analysis Manual for Midas GEN. 2020.

Pennucci, D., Calvi, G.M., Sullivan, T.J. (2009). Displacement-based design of precast walls with additional dampers, *Journal Earthquake Engineering*, 13(S1):40□65. Doi:10.1080/13632460902813265.

Perez, F.J, Pessiki, S., Sause R. (2013). Experimental lateral load response of unbonded post-tensioned precast concrete walls, *ACI Structural Journal*, 110(6):1045-1055.

Pollino, M. (2015). Seismic design for enhanced building performance using rocking steel braced frames, *Eng Struct*, 83: 129-139. Doi:10.1016/j.engstruct.2014.11.005.

Rahman, A.M., Restrepo, J.I. (2000). Earthquake Resistant Precast Concrete Buildings: Seismic Performance of Cantilever Walls Prestressed Using Unbonded Tendons, *Research report 0110-3326,* Christchurch, New Zealand, University of Canterbury.

Restrepo, J.I., Rahman, A. (2007). Seismic performance of self-centering structural walls incorporating energy dissipators, *Journal of Structural Engineering*, 133(11):1560□1570. Doi:10.1061/(ASCE)0733-9445(2007)133:11(1560).

Schoettler, M.J., Belleri, A., Zhang, D., Restrepo, J.I., Fleishman, R.B. (2009). Preliminary results of the shake-table testing for the development of a diaphragm seismic design methodology, *PCI Journal*, 54(1):100-124.

Sivaselvan, M. V., & Reinhorn, A. M. (2006). Lagrangian approach to structural collapse simulation. Journal of Engineering mechanics, 132(8), 795-805.

Tremblay, R., Poirier, L., Bouaanani, N., Leclerc, M., Rene, V., Fronteddu, L., Rivest, S. (2008). Innovative viscously damped rocking braced steel frames, *14th World Conference on Earthquake Engineering,* Beijing, China.